Effects of Fused-Ring Regiochemistry on the Properties and Photovoltaic Performance of n-type Organic Semiconductor Acceptors

Effects of Fused-Ring Regiochemistry on the Properties and Photovoltaic Performance of *n*-type Organic Semiconductor Acceptors

Xiaojun Li,[a b] He Huang,[b] Zhengxing Peng,[c] Chenkai Sun,[a b] Dengchen Yang,[a] Jiadong Zhou,[e] Alex Liebman-Pelaez,[d] Chenhui Zhu,[d] Zhi-Guo Zhang,[a] Zhanjun Zhang,[b] Zengqi Xie,[e] Harald Ade,[c] *Yongfang Li[a b f] *

[a] CAS Research/Education Center for Excellence in Molecular Sciences, CAS Key Laboratory of Organic Solids, Institute of Chemistry, Chinese Academy of Sciences, Beijing 100190, China;

[b] School of Chemical Science, University of Chinese Academy of Sciences, Beijing 100049, China;

[c] Department of Physics and Organic and Carbon Electronics Lab (ORaCEL), North Carolina State University, Raleigh, North Carolina 27695, USA;

[d] Advanced Light Source, Lawrence Berkeley National Laboratory, Berkeley, California 94720, USA.

[e] Institute of Polymer Optoelectronic Materials and Devices, State Key Laboratory of Luminescent Materials and Devices, South China University of Technology, Guangzhou 510640, China.

[f] Laboratory of Advanced Optoelectronic Materials, College of Chemistry, Chemical Engineering and Materials Science, Soochow University, Suzhou, Jiangsu 215123, China;

*Email - liyf@iccas.ac.cn

Abstract

The effects of fused-ring regiochemistry on the physicochemical and photovoltaic properties of n-type organic semiconductor (n-OS) acceptors are investigated. Two n-OS isomers TPTC and TPTIC were prepared with different oxygen positions in the central fused-ring unit of the acceptor molecules: oxygen is connected with benzene in TPTC and it is connected with two thiophenes in TPTIC. It is found that TPTC tends to form excessive self-aggregation with several different packing motifs or polymorphs, while TPTIC with compact alkyl chains forms well-defined crystals. The electron mobility of TPTC, which is measured by the space-charge-limited current (SCLC) method, is much lower than that of TPTIC. When blending these acceptors with the polymer PTQ10, excessive self-aggregation of TPTC leads to large phase separation and exhibits little change after thermal annealing treatment, while the intermolecular interaction in TPTIC is appropriate to form suitable phase separation in its blend films with PTQ10, and the stacking of both crystallites were obviously improved after thermal annealing. Thus the PSCs with TPTIC as the acceptor show much higher power conversion efficiency (PCE) of 10.42%, in comparison with that (1.97%) of the device with TPTC as acceptor. These results indicate that the regiochemistry of the n-OS acceptors greatly influences the aggregation behavior of the molecules, so that strongly affects the performance of the PSCs, and the structure-property relationship of the materials with the regiochemistry could guide the development of high performance n-OS acceptors.

In recent years, polymer solar cells (PSCs) have drawn considerable attention as an emerging energy conversion technology, and the power conversion efficiencies (PCEs) of the PSCs have reached over 14%[1-4]. This progress has greatly benefitted from the development of the low bandgap acceptor-donor-acceptor

(A-D-A)-structured *n*-type organic semiconductor (*n*-OS) acceptors[5-12] and the structure optimization of polymer donors which are absorption-complementary and energy level matching with the acceptors[13-19]. In the A-D-A type *n*-OS acceptors, the fused-ring aromatic building blocks were widely used as the central donor unit[20-27]. Such fused rings feature high thermal, chemical and mechanical stabilities. Furthermore, their planar rigid backbone strengthens the π-orbital interactions, elongates the effective conjugation length and facilitates π-electron delocalization. Moreover, these coplanar structures effectively suppress the rotation of adjacent rings to lower reorganization energy, which is beneficial to enhance the intrinsic charge mobility[26, 28, 29]. Owing to the superior inherent structural characteristics, the fused-ring-based molecules (such as IDT or IDTT-based small molecules) are state-of-the-art *n*-OS acceptors and widely used in high-efficiency PSCs. However, for these fused-ring-based molecules, the good planarity and large conjugation length can also lead to excessive self-aggregation and large phase separation. In order to obtain desirable *n*-OS acceptors that can match with donors to achieve favorable morphology, flexible side chains should be introduced to improve their solubility and to tune the morphology of their blend films with polymer donor for obtaining good photovoltaic performance.

Side-chain engineering is one of the commonly used strategies to tune solubility, aggregation behavior and intermolecular interactions of the donor and acceptor materials for improving their photovoltaic performance[19, 30-32]. Nowadays, most of the related studies were focused on optimizing side-chain lengths, geometry, or introducing alkyloxy or conjugated side chains[30, 33-35], while the effects of side chain regiochemistry were not yet systematically studied for the fused-ring *n*-OS acceptors[36]. The fused-ring regiochemistry of the *n*-OS acceptors could provide new knowledge on the structure-property relationship for further improving photovoltaic performance of the *n*-OS acceptors.

In this work, we synthesized two fused-ring *n*-OS isomers TPTC and TPTIC with different oxygen positions in the fused-ring central donor units of the acceptors[29, 37, 38]. Oxygens of the crosslinked alkoxy side chains are connected with benzene in

TPTC and they are connected with two thiophenes in TPTIC. Meanwhile, the side chains of these two molecules are located in different regions on the central donor unit along with different positions of oxygen atoms in the structure. Then the effects of the different regiochemistry on the physicochemical and photovoltaic properties of the acceptors were studied systematically. It was found that TPTIC shows more appropriate aggregation behavior and high electron mobility than that of TPTC. Photovoltaic properties of the two acceptors demonstrated big difference with the PCE values of 1.97% and 10.42% for the PTQ10-based PSCs with TPTC and TPTIC as acceptor respectively. The results indicate that regiochemistry is another important strategy to regulate the aggregation and photovoltaic properties of the *n*-OS acceptors.

Scheme 1. Synthetic routes of TPTC and TPTIC. Reagents and conditions: i) Pd(OAc)$_2$, acetone, NaOH (aq); ii) BBr$_3$, CH$_2$Cl$_2$, rt.; iii) *n*-octylmagnesium bromide, THF, rt.; *p*-toluenesulfonic acid, toluene, reflux; iv) POCl$_3$, DMF, CHCl$_3$, reflux; v) 1,1-dicyanomethylene-3-indanone, pyridine, CHCl$_3$, reflux.

Synthetic routes of the isomers TPTC and TPTIC are shown in Scheme 1, and the detailed synthetic procedures are described in the Supporting Information (SI). Compound **1** and Compound **2** were synthesized according to the literatures[39]. Intermediate **3** was prepared by Suzuki reaction of **1** and **2** using Pd(OAc)$_2$ as catalyst at rt. and crude product was purified directly by washing with methanol. Then product **3** was dissolved in dry CH$_2$Cl$_2$ and then reacted with BBr$_3$. After being stirred at rt. for

12h, water was added and the precipitation was filtered. After dried, the precipitated compound **4** was dissolved in dry THF and reacted with *n*-octylmagnesium bromide. The crude product without further purification was dissolved in toluene and reacted with *p*-toluenesulfonic acid monohydrate giving product **5** in high yields. Then the intermediate **6** was prepared by Vilsmeier-Haack reaction of **5** with $POCl_3$ in DMF. Subsequently, target molecules TPTC and TPTIC were synthesized by Knoevenagel condensation of **6** with 1,1-dicyanomethylene-3-indanone (IC) in high yield (85% for TPTC and 89% for TPTIC) as dark blue solids. All the compounds were fully characterized by conventional NMR and mass spectroscopy. The thermogravimetric analysis indicates that TPTC and TPTIC are thermally stable at up to 328 and 317 °C respectively. (5 wt% loss, Figure S1 in Supporting Information (SI)).
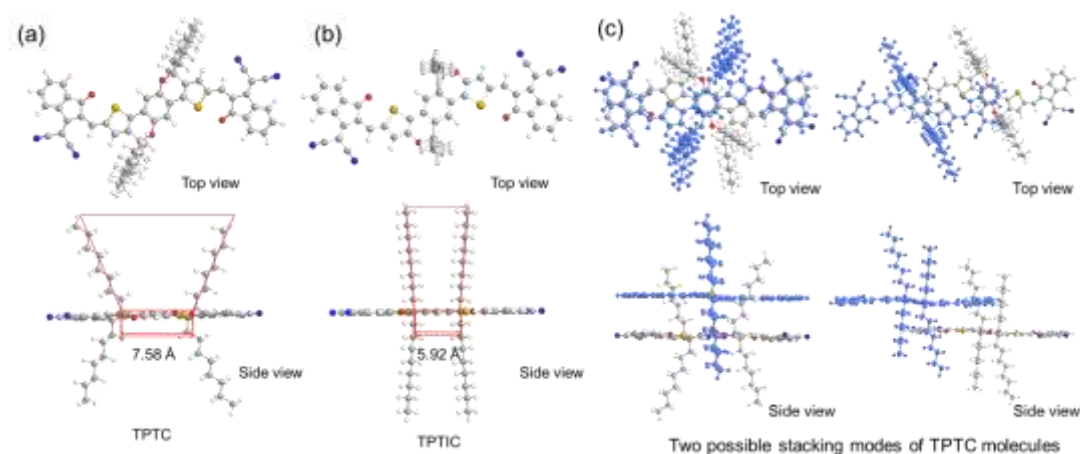

Figure 1. Optimized molecular geometries of (a) TPTC, (b) TPTIC by DFT calculation at the B3LYP/6-31 G (d,p) level. (c) Schematic illustration of two possible stacking modes of TPTC.

In order to reveal the essential difference between the two molecules in the stereoscopic structure, DFT calculation is carried out at the B3LYP/6-31 G (d, p) level on the Gaussian 09 package to evaluate the optimal geometric configurations for TPTC and TPTIC, as shown in Figure 1. Clearly, both TPTC and TPTIC present nearly flat conformations. The difference between these two molecules is mainly in the geometric configuration, especially in the spatial position of the alkyl chain. TPTC exhibits a relatively longer distance of 7.58 Å while TPTIC has a shorter distance of

5

5.92 Å between the two side chains (Figure 1a, b). The different molecular geometry of the two *n*-OS acceptors could influence their aggregation behavior and photovoltaic performance. In ITIC derivatives, the electron-rich central unit is not involved in π-π interactions due to the steric hindrance of the side groups. It is the electron deficient end units that form π-π interactions with the polymer donors or the adjacent acceptor molecules in their blend films, which facilitates efficient electron transfer and transport[40, 41]. As for TPTC and TPTIC, the more compact alkyl chains of TPTIC lead to the suppression of π-π stacking between their electron-rich cores, as shown in Figure S2 in SI. While the relatively small steric hindrance of the side chains in TPTC results in more complicated π-π stacking and more diversified aggregation modes, as shown in Figure 1c and Figure S3 in SI, which may result in complicated aggregation morphology detrimental to the electrons separation and transportation.
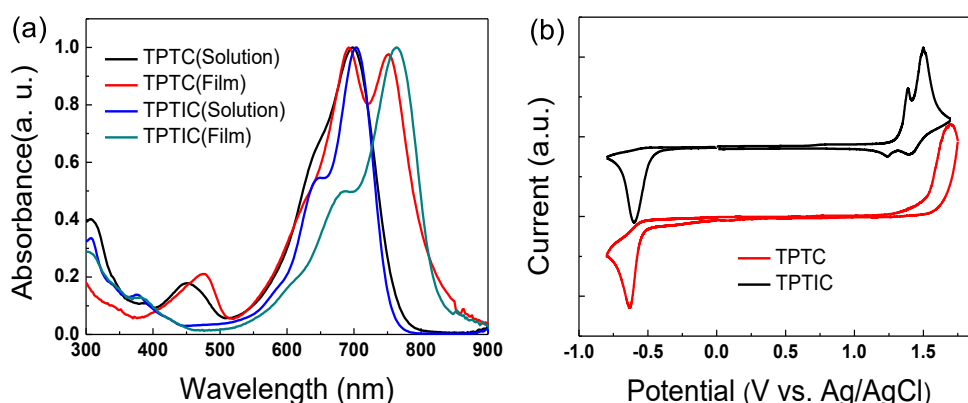

Figure 2. (a) Absorption spectra of TPTC and TPTIC in chloroform solutions and film state. (b) Cyclic voltammograms of TPTC and TPTIC.

The UV-vis absorption spectra of the two isomers in solutions and films (without thermal annealing) are shown in Figure 2a. For TPTC and TPTIC, the absorption spectral ranges are similar in solution (from 550 nm to 800 nm) with the maximum extinction coefficient of 1.1×10^5 and 1.5×10^5 M^{-1} cm^{-1} at 699 and 703 nm, respectively. In addition, TPTIC shows an obvious shoulder peak, indicating its stronger aggregation than TPTC in solution. The film absorption spectra of the

molecules are significantly redshifted in comparison with their solutions, the maximum absorption of TPTC and TPTIC films were red-shifted from 698 to 750 nm and from 703 to 765 nm, respectively, which indicates that more ordered aggregation and stronger π-π stacking interactions exist in the films of the molecules. The difference between the absorption spectra of TPTC and TPTIC in the range of 400-500 nm may be due to the difference in the position of oxygen atoms. The optical band gap of TPTC and TPTIC films are 1.52 and 1.49 eV respectively, estimated from their absorption edge (818 nm for TPTC and 835 nm for TPTIC).

In order to further investigate the effect of side chain regiochemistry on the properties of the isomers, the UV-vis absorption spectra of the two isomers films before and after thermal annealing (at 120 °C for 5 min) were compared, as shown in Figure S4 in SI. It can be seen that the thermal annealing treatment exhibits different effects on TPTC and TPTIC. The absorption peak of TPTC film has no obvious change before and after the thermal annealing, which indicates that there is no aggregation change in the TPTC film with the thermal annealing. Interestingly, the absorption spectrum of TPTIC film shows broadened absorption band with a new vibrational peak and *ca.* 10 nm red shift after the thermal annealing (see Figure S4b), which suggests that there is further ordered aggregation of TPTIC during the thermal annealing. The new vibrational peak could be ascribed to the enhanced π−π interaction in the ordered aggregation of TPTIC after the thermal annealing. This phenomenon is probably due to the different packing modes of the two molecules, which will be discussed later.

Table 1. Physicochemical Properties of the Two Isomer *n*-OS Accepters.

	λ_{max}[a] (nm)	λ_{edge}[a] (nm)	E_g^{opt}[b] (eV)	E_{HOMO}[c] (eV)	E_{LUMO}[c] (eV)
TPTC	750	818	1.52	-5.85	-3.83
TPTIC	763	835	1.49	-5.67	-3.89

[a] Absorption of the films. [b] Calculated from the absorption edge of the polymer films: $E_g^{opt} = 1240/\lambda_{edge}$. [c] Calculated according to the equation $E_{LUMO/HOMO} = -e (E_{red/ox} + 4.36)$ (eV)

The electronic energy levels of TPTC and TPTIC were measured by

electrochemical cyclic voltammetry, as shown in Figure 2b. The highest occupied molecular orbital (HOMO) and the lowest unoccupied molecular orbital (LUMO) of the two molecules were estimated from the onset oxidation and reduction potentials obtained from their cyclic voltammograms, according to the equations: $E_{HOMO/LUMO} = $ -e ($E_{ox/red}$ + 4.36) (eV). (Redox potential of Fc/Fc$^+$ is 0.44 V *vs* Ag/AgCl in our measurement system, and we take the energy level of Fc/Fc$^+$ as 4.8 eV below vacuum). TPTC has an up-shifted LUMO (-3.83 eV) energy levels and down-shifted HOMO (-5.85 eV) than that (-3.89 eV/-5.67eV) of TPTIC (see Table 1), which could be ascribed to the position effects of oxygen atoms in the isomers.
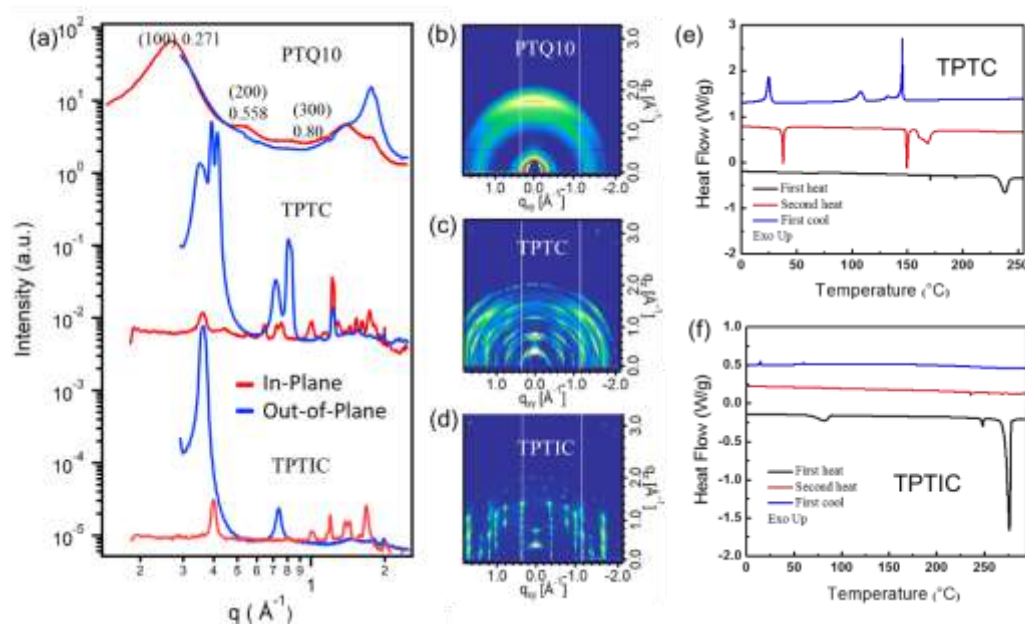

Figure 3. (a) Line cuts of the GIWAXS patterns of PTQ10, TPTC and TPTIC films; 2D GIWAXS patterns of (b) PTQ10 film (c) TPTC film and (d) TPTIC film; DSC plot of (e)TPTC and (f)TPTIC.

Molecular packing of pure films of the two isomers were investigated by grazing-incidence wide-angle X-ray scattering (GIWAXS). As shown in Figure 3, GIWAXS plots indicate both TPTC and TPTIC exhibit highly ordered molecular packing with sharp peaks and strong peak intensities. Neat TPTC film tends to form edge-on orientated crystallites with (100) peak at ~0.4 Å^{-1}, (200) peak at ~0.8 Å^{-1} and (300) peak at ~1.2 Å^{-1} in the OOP. And TPTIC film also tends to form edge-on

orientated crystallites with (100) peak at 0.362 Å^{-1} and (200) peak at 0.737 Å^{-1} in the out-of-plane (OOP). Owing to the different position of the side chains relative to the fused rings, the 2D GIWAXS patterns of TPTC and TPTIC exhibit significant difference. For TPTC, more than one set of (h00) scattering peaks are observed in Figure 2c, suggesting that TPTC may adopt several different packing motifs or polymorphs. The results of GIWAXS indicate that such small change in the side chains has significant influence on the aggregation and molecular ordering in the neat films of the isomers, which could affect the photovoltaic performance of the *n*-OS acceptors.

For further investigating the difference in aggregation between the two isomers, the differential scanning calorimetry (DSC) was measured, as shown in Figure 3(e,f). In the first heating of the DSC measurement, the two isomers both display obvious melting peak, revealing that there are crystallite structures in the two films prepared by dropcast from their solutions. TPTC shows a higher melting temperature (289.5℃) and melting enthalpy (49.23 J/g) than that of TPTIC (276.3℃ and 38.00 J/g), indicating that more energy is needed for the TPTC film to break the crystallite structure. This might also contribute to the different responses to thermal annealing of the two molecules. The TPTIC formed well-defined crystals and can be further promoted by the thermal annealing, while TPTC forms a vast amount of compact crystals (Figure 6), and the packing is hard to break, thus no further growth of crystals is observed during thermal annealing. Besides, it is interesting to note that, at the 2nd heating, there is no melting peak for TPTIC, while TPTC still shows some peaks. This indicates that the crystallization is highly suppressed when cooled at 10 °C/min from the melt and the crystallization is facilitated by the initial presence of the solvent. Collectively, the data above suggest different crystallization behavior of the two isomers, which is consistent with what is observed in the GIWAXS measurement.

In order to compare the difference in the charge transporting properties of the isomers, electron mobilities of the two isomers were measured by the space-charge-limited current (SCLC) method with electron only device of ITO/ZnO/active layer/PDINO/Al. Figure S6 in SI shows the results. The calculated

electron mobility of TPTIC is 1.83×10^{-4} cm^2 V^{-1} s^{-1}, which is much higher than that (0.33×10^{-4} cm^2 V^{-1} s^{-1}) for TPTC.
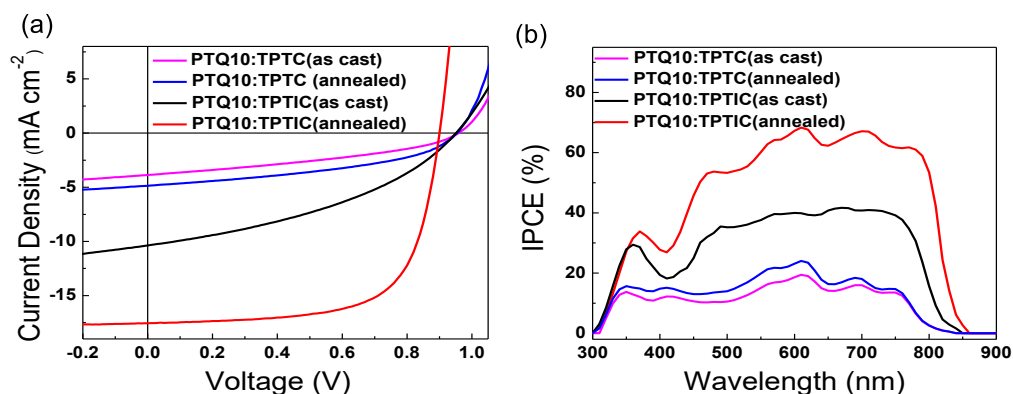

Figure 4. (a) $J-V$ curves of the optimized PSCs with D/A weight ratio of 1:1.5 without (as-cast) and with thermal annealing at 120 °C for 5 min under the illumination of AM 1.5G, 100 mW cm^{-2}; (b) IPCE spectra of the corresponding PSCs.

All these results of optical properties, electronic energy levels, crystallinity and electron mobilities show that the regiochemistry of the fused-ring central unit can have significant impacts on the properties of the *n*-OS isomers. In order to further investigate the influences of the regiochemistry on the photovoltaic performance of the isomers, the PSCs with a conventional configuration of ITO/PEDOT: PSS/PTQ10: acceptors (TPTC or TPTIC)/PDINO/Al were fabricated, in which medium bandgap conjugated polymer PTQ10 was used as the electron donor[17], PEDOT: PSS and PDINO performed as the anode and cathode electrode buffer layers, respectively. Device fabrication details are described in the Supporting Information. The donor/acceptor (D/A) weight ratio in the active layer of the devices was optimized to be 1:1.5. Figure 4 shows the current density-voltage (*J-V*) curves and input photon to converted current efficiency (IPCE) spectra of the PSCs, and Table 2 lists the photovoltaic performance parameters of the devices for a clear comparison. The PSC based on PTQ10:TPTC without thermal annealing showed a very low PCE of 1.36%, even after the annealing treatment, the PCE of the TPTC-based PSC is only a little improved to 1.97%, due to its lower J_{sc} and FF. While under the same processing conditions and the same PTQ10 batch, the as-cast device based on PTQ10:TPTIC

delivered a PCE of 3.83% with a V_{oc} of 0.95 V, J_{sc} of 10.38 mA/cm^2, and FF of 38.79%. After optimization with thermal annealing at 120 ^{o}C for 5 min, the TPTIC-based PSCs demonstrated a PCE of 10.42 % with a V_{oc} of 0.90 V, J_{sc} of 17.17 mA/cm^2, and FF of 67.45 %. The big difference of the photovoltaic performance of the two isomer acceptors could be due to their different aggregation behavior in the blend active layers of the PSCs.

Table 2. Photovoltaic Performance Parameters of the PSCs Based on PTQ10/acceptors (1:1.5, w/w) under the illumination of AM1.5G, 100 mW/cm^2

Acceptor	V_{oc} (V)	J_{sc} (mA cm^{-2})	FF (%)	PCE (%)	calculated J_{sc} from IPCE (mA cm^{-2})
TPTC[a]	0.96	3.87	36.69	1.36	3.67
TPTC[b]	0.95	4.87	42.56	1.97	4.65
TPTIC[a]	0.95	10.38	38.79	3.83	9.60
TPTIC[b]	0.90	17.17	67.45	10.42	16.44

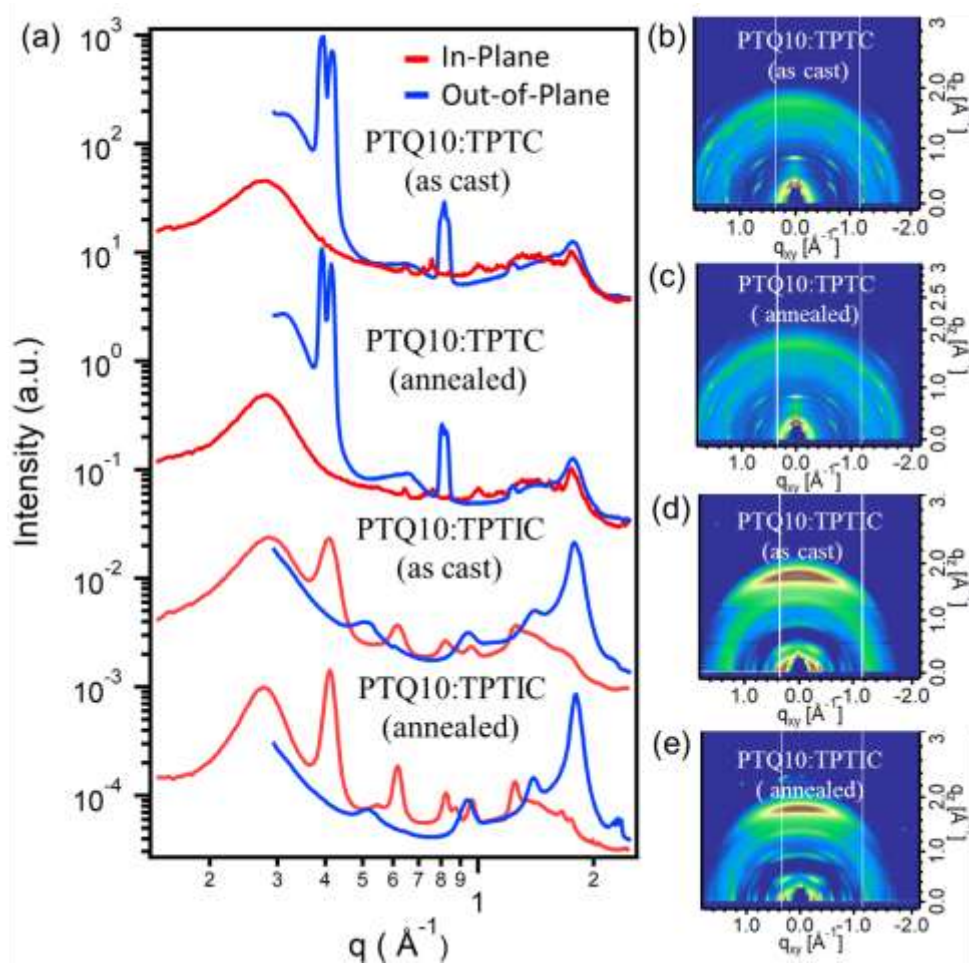a) Without thermal annealing; b) With thermal annealing at 120 °C for 5 min.

Figure 5. (a) Line cuts of GIWAXS patterns of the as cast PTQ10/acceptors blend films and annealed blend films. 2D GIWAXS patterns of (b) as cast PTQ10/TPTC blend films; (c) annealed PTQ10/TPTC blend films; (d) as cast PTQ10/TPTIC blend films; (e) annealed PTQ10/TPTIC blend films. (where "annealed" means "with thermal annealing at 120 °C for 5 min ")

In order to gain a deeper understanding about the influence of the regiochemistry on the device performance, we conducted GIWAXS[42] measurements on the blend films, from which the detailed morphology information such as molecular packing and orientation in the blend films can be extracted. In the GIWAXS pattern of PTQ10:TPTC blend film (Figure 5a), the π-π stacking peak is shown in both IP and OOP, suggesting that there are both face-on and edge-on crystallites. Furthermore, in the TPTC-based film, PTQ10 and TPTC still maintain their independent and unchanged crystallinity, exhibiting two polymorphs similar to those observed in the

pure films. After thermal annealing, there is little change in their aggregation behavior of the PTQ10:TPTC blend films, the π-π stacking distance and OOP coherence length didn't change much. While the TPTIC crystallites of its blend films show a face-on orientation with the (100) peak at 0.408 A^{-1} in the in-plane (IP) comparing to the edge-on orientation with the (100) peak at 0.362 $Å^{-1}$ in the neat film. The (100) peak of PTQ10 moves to 0.288 A^{-1} from 0.271 A^{-1} in neat PTQ10 film, and (100) peak of TPTIC moves to 0.408 A^{-1} from 0.362 A^{-1} in neat TPTIC film, which suggests a closer packing in both PTQ10 and TPTIC crystallites in the blend films. In addition, after thermal annealing, significantly stronger and sharper peaks, especially π-π stacking peak, are observed in the PTQ10: TPTIC film. Although π-π stacking distance maintains unchanged, it exhibits higher OOP coherence length (from 38.7 to 54.6 Å), which is beneficial for charge transport in vertical direction. Meanwhile, the RSoXS results (Figure S8 in SI) indicate that the purity of the domains is higher in the as-cast samples of these two blend films than that in the thermal-annealed samples, and the highly pure domains may result in more trapped charges and slightly lower J_{sc} and FF[43] values. The origins of the difference between the PTQ10:TPTC and PTQ10:TPTIC blend films could be due to the different interactions of these two isomer acceptors with the PTQ10 donor leading to stronger vitrification, or attributed to the intrinsic aggregation properties of the two acceptors.

Optical microscopy was used to obtain the morphological images for the blend films of PTQ10:TPTC or TPTIC and the neat films of TPTC, TPTIC (Figure 6). In Figure 6a, the blend film of PTQ10 with TPTC exhibits obviously crystalline particles, however the film based on TPTIC shows a smooth surface (Figure 6b). A large number of compact crystals were also observed in the neat film of TPTC (Figure 6c). These results indicate that the large crystal of TPTC-based blend film is due to the intrinsic aggregation properties of the acceptor, rather than the different interactions between donor and acceptor components, which determines the large phase separation of the neat and blend films. The surface and bulk morphology of PTQ10: TPTC or TPTIC blend films were also studied by atomic force microscopy (AFM) and transmission electron microscopy (TEM). As shown in Figure S7 in SI, the film based

on TPTIC exhibits a uniform and smooth surface, the corresponding TEM images exhibit finely dispersed phase separation. However, for the TPTC-based blend films, the strong aggregation was observed in AFM, and TEM results show that the TPTC tends to form large phase separation. With these results, it is likely that the PTQ10:TPTC blend suffered from excessively large phase separation, which results in its poor J_{sc} and lower IPCE, as a large portion of excitons generated in the PTQ10:TPTC blend cannot diffuse to the interfaces for charge separation but will recombine to ground states[44]. In summary, the morphological results indicate that the intermolecular interaction in TPTIC is appropriate to form suitable nano-scaled phase separation in its blend films with PTQ10 donor, while the larger aggregates of TPTC inhibited the mixing and induced large phase separation with PTQ10, so that serious phase separation exited in the active layer of the TPTC-based PSCs. It is the different morphology of the acceptor isomers that influenced their photovoltaic performance.
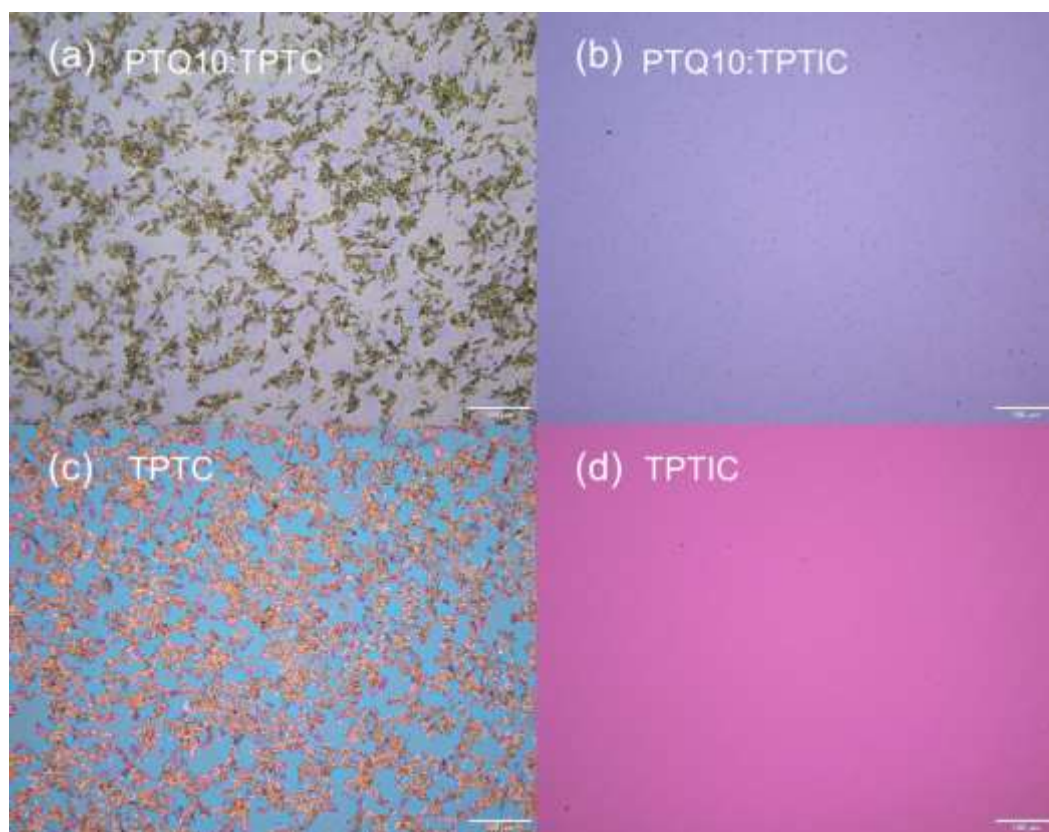

Figure 6. Optical microscopy images of (a) PTQ10:TPTC blend film, (b) PTQ10: TPTIC blend film, (c) TPTC neat film, (d) TPTIC neat film.

In conclusion, the effects of the fused-ring regiochemistry on the physicochemical and photovoltaic performance of the two *n*-OS acceptor isomers are investigated. The different positions of oxygen and side chains on the fused-ring central units have significant impact on the steric hindrance, intermolecular interactions and aggregation behavior of the acceptors, thus resulting in significant effect on the active layer morphology, their absorption spectra, electron mobility and photovoltaic performance. TPTIC possesses higher electron mobility and forms appropriate aggregation in its blend films with PTQ10 donor, especially after thermal annealing, while TPTC has lower electron mobility and excessive phase separation in its blend films with PTQ10. As a result, the PSCs based on TPTIC yielded a high PCE up to 10.42%, while the PCE of the TPTC-based PSCs was only 1.97%. These results indicate that the regiochemistry of the fused-ring central units greatly influences the photovoltaic performance of the *n*-OS acceptors, and the structure-property relationship could guide the development of the *n*-OS acceptors for high performance PSCs.

Conflicts of interest: There are no conflicts of interest to declare.

Acknowledgements

Author Contributions: X. L. designed, synthesized and characterized the *n*-type organic semiconductor acceptors. H. H. carried out fabrication and characterization of the PSCs. C. S. provided the polymer PTQ10. D. Y. participated in the DFT calculation. Z. P., A. L.-P., C. Z. and H. A. measured the GIWAXS diffraction patterns and the DSC results. J. Z. and Z. X. provided the crystal structure of TPTC. Z.G. Z. and Z.J. Z. participated discussion of the results, Y. L. supervised the project. X. L. and Y. L. wrote the paper.

References

1. (a) W. Zhao, S. Li, H. Yao, S. Zhang, Y. Zhang, B. Yang and J. Hou, *J. Am. Chem. Soc.*, 2017, **139**, 7148. (b) S. Zhang, Y. Qin, J. Zhu and J. Hou, *Adv. Mater.*, 2018, **30**, 1800868. (c) S. Li, L. Ye, W. Zhao, H. Yan, B. Yang, D. Liu, W. Li, H. Ade and J. Hou, *J. Am. Chem. Soc.*, 2018, **140**, 7159.

2. Z. Fei, F. D. Eisner, X. Jiao, M. Azzouzi, J. A. Rohr, Y. Han, M. Shahid, A. S. R. Chesman, C. D. Easton, C. R. McNeill, T. D. Anthopoulos, J. Nelson and M. Heeney, *Adv. Mater.*, 2018, **30**, 1705209.

3. J. Sun, X. Ma, Z. Zhang, J. Yu, J. Zhou, X. Yin, L. Yang, R. Geng, R. Zhu, F. Zhang and W. Tang, *Adv. Mater.*, 2018, **30**, 1707150.

4. Q. Fan, W. Su, Y. Wang, B. Guo, Y. Jiang, X. Guo, F. Liu, T. P. Russell, M. Zhang and Y. F. Li, *Sci. China Chem.*, 2018, **61**, 531.

5. (a) S. Dai, F. Zhao, Q. Zhang, T. K. Lau, T. Li, K. Liu, Q. Ling, C. Wang, X. Lu, W. You and X. Zhan, *J. Am. Chem. Soc.*, 2017, **139**, 1336. (b) B. Jia, Y. Wu, F. Zhao, C. Yan, S. Zhu, P. Cheng, J. Mai, T.-K. Lau, X. Lu, C.-J. Su, C. Wang and X. Zhan, *Sci. China Chem.*, 2017, **60**, 257. (c) S. Li, L. Ye, W. Zhao, S. Zhang, H. Ade and J. Hou, *Adv. Energy Mater.*, 2017, **7**, 1700183.

6. Y. T. Hsiao, C. H. Li, S. L. Chang, S. Heo, K. Tajima, Y. J. Cheng and C. S. Hsu, *ACS. Appl. Mater. Interfaces*, 2017, **9**, 42035.

7. B. Kan, J. Zhang, F. Liu, X. Wan, C. Li, X. Ke, Y. Wang, H. Feng, Y. Zhang, G. Long, R. H. Friend, A. A. Bakulin and Y. Chen, *Adv. Mater.*, 2017, **29**, 1704904.

8. (a) X. Li, H. Huang, H. Bin, Z. Peng, C. Zhu, L. Xue, Z.-G. Zhang, Z. Zhang, H. Ade and Y. F. Li, *Chem. Mater.*, 2017, **29**, 10130. (b) X. Li, T. Yan, H. Bin, G. Han, L. Xue, F. Liu, Y. Yi,

Z.-G. Zhang, T. P. Russell and Y. F. Li, *J. Mater. Chem. A*, 2017, **5**, 22588. (c) X. Zhang, J. Yao and C. Zhan, *Sci. China Chem.*, 2016, **59**, 209.

9.   (a) Y. X. Li, L. Zhong, B. Gautam, H.-J. Bin, J.-D. Lin, F.-P. Wu, Z. Zhang, Z.-Q. Jiang, Z.-G. Zhang, K. Gundogdu, Y. F. Li and L.-S. Liao, *Energy Environ. Sci.*, 2017, **10**, 1610. (b) J. Jia, N. Zheng, Z. Wang, Y. Huang, C. Duan, F. Huang and Y. Cao, *Sci. China Chem.*, 2017, **60**, 1458.

10. W. Liu, J. Zhang, Z. Zhou, D. Zhang, Y. Zhang, S. Xu and X. Zhu, *Adv. Mater.*, 2018, **30**, 1800403.

11. (a) W. Gao, M. Zhang, T. Liu, R. Ming, Q. An, K. Wu, D. Xie, Z. Luo, C. Zhong, F. Liu, F. Zhang, H. Yan and C. Yang, *Adv. Mater.*, 2018, **30**, 1800052. (b) Z. Luo, H. Bin, L. Tao, Z.-G. Zhang, Y. K. Yang, C. Zhong, B. Qiu, G. Li, W. Gao, D. Xie, K. Wu, Y. Sun, F. Liu, Y. F. Li and C. Yang, *Adv. Mater.,* 2018, **30**, 1706124.

12. D. Baran, R. S. Ashraf, D. A. Hanifi, M. Abdelsamie, N. Gasparini, J. A. Rohr, S. Holliday, A. Wadsworth, S. Lockett, M. Neophytou, C. J. Emmott, J. Nelson, C. J. Brabec, A. Amassian, A. Salleo, T. Kirchartz, J. R. Durrant and I. McCulloch, *Nat. Mater.*, 2017, **16**, 363.

13. (a) G. Zhang, X. Xu, Z. Bi, W. Ma, D. Tang, Y. Li and Q. Peng, *Adv. Funct. Mater.*, 2018, **28**, 1706404. (b) X. Xu, Z. Li, Z. Bi, T. Yu, W. Ma, K. Feng, Y. Li and Q. Peng, *Adv. Mater.*, 2018, **30**, 1800737.

14. B. Fan, K. Zhang, X. F. Jiang, L. Ying, F. Huang and Y. Cao, *Adv. Mater.*, 2017, **29**. 1606396.

15. B. Guo, W. Li, X. Guo, X. Meng, W. Ma, M. Zhang and Y. F. Li, *Adv. Mater.*, 2017, **29**. 1702291.

16. Z. Li, K. Jiang, G. Yang, J. Y. Lai, T. Ma, J. Zhao, W. Ma and H. Yan, *Nat. commun.*, 2016, **7**, 13094.

17. C. Sun, F. Pan, H. Bin, J. Zhang, L. Xue, B. Qiu, Z. Wei, Z. G. Zhang and Y. F. Li, *Nat. commun.*, 2018, **9**, 743.

18. Q. Fan, Y. Wang, M. Zhang, B. Wu, X. Guo, Y. Jiang, W. Li, B. Guo, C. Ye, W. Su, J. Fang, X. Ou, F. Liu, Z. Wei, T. C. Sum, T. P. Russell and Y. F. Li, *Adv. Mater*., 2018, **30**, 1704546.

19. (a) H. Bin, L. Gao, Z. G. Zhang, Y. Yang, Y. Zhang, C. Zhang, S. Chen, L. Xue, C. Yang, M. Xiao and Y. F. Li, *Nat. commun.*, 2016, **7**, 13651. (b) S. Feng, Cai. Zhang, Y. Liu, Z. Bi, Z. Zhang, X. Xu, W. Ma and Z. Bo, *Adv. Mater.,* 2017, **29**, 1703527.

20. Y. Lin, J. Wang, Z. G. Zhang, H. Bai, Y. F. Li, D. Zhu and X. Zhan, *Adv. Mater.*, 2015, **27**, 1170.

21. Y. Lin, Q. He, F. Zhao, L. Huo, J. Mai, X. Lu, C. J. Su, T. Li, J. Wang, J. Zhu, Y. Sun, C. Wang and X. Zhan, *J. Am. Chem. Soc.*, 2016, **138**, 2973.

22. B. Kan, H. Feng, X. Wan, F. Liu, X. Ke, Y. Wang, Y. Wang, H. Zhang, C. Li, J. Hou and Y. Chen, *J. Am. Chem. Soc.*, 2017, **139**, 4929.

23. Y. Ma, M. Zhang, Y. Yan, J. Xin, T. Wang, W. Ma, C. Tang and Q. Zheng, *Chem. Mater.*, 2017, **29**, 7942.

24. N. Qiu, H. Zhang, X. Wan, C. Li, X. Ke, H. Feng, B. Kan, H. Zhang, Q. Zhang, Y. Lu and Y.

Chen, *Adv. Mater.*, 2017, **29**,1604964.

25. W. Wang, C. Yan, T. K. Lau, J. Wang, K. Liu, Y. Fan, X. Lu and X. Zhan, *Adv. Mater.*, 2017, **29**, 1701308.

26. H. Wu, H. Fan, S. Xu, C. Zhang, S. Chen, C. Yang, D. Chen, F. Liu and X. Zhu, *Solar RRL*, 2017, **1**, 1700165.

27. S. J. Xu, Z. Zhou, W. Liu, Z. Zhang, F. Liu, H. Yan and X. Zhu, *Adv. Mater.*, 2017, **29**, 1704510.

28. Y. X. Xu, C. C. Chueh, H. L. Yip, F. Z. Ding, Y. X. Li, C. Z. Li, X. Li, W. C. Chen and A. K. Jen, *Adv. Mater.*, 2012, **24**, 6356.

29. T. Qin, Y. Zang, W. Y. Bai, K. Yao and Y. X. Xu, *Macromol. Rapid Commun.*, 2017, **38**, 1700156.

30. Y. Yang, Z. G. Zhang, H. Bin, S. Chen, L. Gao, L. Xue, C. Yang and Y. F. Li, *J. Am. Chem. Soc.*, 2016, **138**, 15011.

31. H. Bin, Z. G. Zhang, L. Gao, S. Chen, L. Zhong, L. Xue, C. Yang and Y. F. Li, *J. Am. Chem. Soc.*, 2016, **138**, 4657.

32. Z.-G. Zhang and Y. F. Li, *Sci. China Chem.*, 2014, **58**, 192.

33. H. Bin, Y. Yang, Z. Peng, L. Ye, J. Yao, L. Zhong, C. Sun, L. Gao, H. Huang, X. Li, B. Qiu, L. Xue, Z.-G. Zhang, H. Ade and Y. F. Li, *Adv. Energy Mater.*, 2018, **8**, 1702324.

34. J. Wang, W. Wang, X. Wang, Y. Wu, Q. Zhang, C. Yan, W. Ma, W. You and X. Zhan, *Adv. Mater.*, 2017, **29**, 1702125.

35. L. Ye, S. Zhang, W. Zhao, H. Yao and J. Hou, *Chem. Mater.*, 2014, **26**, 3603.

36. (a) S. Chen, L. Zhang, C. Ma, D. Meng, J. Zhang, G. Zhang, Z. Li, P. C. Y. Chow, W. Ma, Z. Wang, K. S. Wong, H. Ade and H. Yan, *Adv. Energy Mater.*, 2018, **8**, 1702427. (b) I.Osaka and R. D. McCullough, *Acc. Chem. Res.,* 2008, **41**, 1202. (c) Y. Huang, N. Zheng, Z. Wang, L. Ying, F. Huang and Y. Cao, *Chem. Commun.,* 2017, **53**, 1997. (d) L. Ying, F. Huang and G. C. Bazan, *Nat. Commun.*, 2018, **8**, 14047.

37. J. You, L. Dou, K. Yoshimura, T. Kato, K. Ohya, T. Moriarty, K. Emery, C. C. Chen, J. Gao, G. Li and Y. Yang, *Nat. commun*, 2013, **4**, 1446.

38. (a) Y. Zhou, M. Li, J. Song, Y. Liu, J. Zhang, L. Yang, Z. Zhang, Z. Bo and H. Wang, *Nano Energy*, 2018, **45**, 10. (b) L. Yang, M. Li, J. Song, Y. Zhou, Z. Bo and H. Wang, *Adv. Funct. Mater.,* 2018, **28**, 1705927.

39. (a) P.-H. Aubert, M. Knipper, L. Groenendaal, L. Lutsen, J. Manca and D. Vanderzande, *Macromolecules*, 2004, **37**, 4087. (b) V. Benin, S. Durganala and A. B. Morgan, *J. Mater. Chem.,* 2012, **22**, 1180.

40. G. Han, Y. Guo, X. Song, Y. Wang and Y. Yi, *J. Mater. Chem. C*, 2017, **5**, 4852.

41. J. Hou, O. Inganas, R. H. Friend and F. Gao, *Nat. Mater.*, 2018, **17**, 119.

42. A. Hexemer, W. Bras, J. Glossinger, E. Schaible, E. Gann, R. Kirian, A. MacDowell, M. Church, B. Rude and H. Padmore, *J. Phys: Conf. Ser.*, 2010, **247**, 012007.

43. (a) E. Gann, A. T. Young, B. A. Collins, H. Yan, J. Nasiatka, H. A. Padmore, H. Ade, A.

Hexemer, and C. Wang, *Rev. Sci. Instrum.,*2012, **83**,045110. (b) L.Ye, B. A. Collins, X. Jiao, J. Zhao, H. Yan, and H. Ade, *Adv. Energy Mater.,* 2018, **8**, 1703058.

44. T. M. Clarke and J. R. Durrant, *Chem. Rev.,* 2010, **110**, 6736.